Chemical-Looping Combustion with NiO and Fe2O3 in a Thermobalance and Circulating Fluidized Bed Reactor with Double Loops

ARTICLE *in* INDUSTRIAL & ENGINEERING CHEMISTRY RESEARCH · MARCH 2006

Impact Factor: 2.59 · DOI: 10.1021/ie050919x

Chemical-Looping Combustion with NiO and Fe_2O_3 in a Thermobalance and Circulating Fluidized Bed Reactor with Double Loops

Sung Real Son and Sang Done Kim*

Department of Chemical and Biomolecular Engineering and Energy and Environment Research Center, Korea Advanced Institute of Science and Technology, Daejeon, 305-701, Korea

For the chemical-looping combustion (CLC), readily available metal oxides (NiO, Fe_2O_3) for oxygen carriers and bentonite, TiO_2, and Al_2O_3 for the supports of the looping materials were selected. The reactivity of the oxygen carrier particles was determined in a thermobalance reactor under the reducing (CH_4) and oxidizing (O_2) conditions at 923−1223 K. The reactivity of NiO is higher than Fe_2O_3, and the particles supported on bentonite or Al_2O_3 produce higher reactivity than those on TiO_2. The reactivity of the metal oxide particles increases with increasing temperature and the amount of NiO. The obtained kinetic data of the NiO−Fe_2O_3/bentonite can be analyzed based on the modified volumetric and shrinking core models for the reduction and oxidation conditions, respectively. The CLC experiment was carried out in an annular shape circulating fluidized bed (CFB) reactor with double loops. To determine the optimum fuel gas velocity, the mixture of NiO and Fe_2O_3 (75:25) on a bentonite support was tested at 1123 K. The CH_4 conversion was higher at lower velocities than that at higher ones, and the optimum CH_4 gas velocity for complete combustion was found to be around 2−3 u_{mf} (minimum fluidizing velocity). Combustion efficiency increases with increasing temperature, and the optimum reaction temperature was found to be around 1123 K. It was found that CO emission from the fuel reactor was negligibly small, and no H_2 emission was detected at the optimum conditions. From the oxidation reactor, NO_x emission was also negligibly small, and CO_2 emission was not detected.

Introduction

It has been known that carbon dioxide (CO_2) is a greenhouse gas that is mainly released from fossil fuel combustion. In developing countries, economic growth results in a rapid increase in demand for an energy supply of fossil fuels, while the means for decreasing the use of these fuels substantially has not yet been found. Soon, it will not be unlikely that radical measures to decrease CO_2 emissions should be implemented.[1]

To remove CO_2 from the flue gas for sequestrating, separation of CO_2 is necessary, and it requires additional equipment using absorption, adsorption, or membrane methods. As over 90% of the cost for CO_2 removal is in the separation processes, the alternative combustion system to separate CO_2 directly from the combustor will be an expensive process. From these demands, reversible combustion was proposed, to utilize oxidation and reduction of the metals,[2] and a novel concept of the chemical-looping combustion (CLC) was proposed.[3] The CLC is an alternative combustion of gas fuel and has the advantage of no energy loss for the separation of CO_2 without nitrogen oxide (NO_x) formation. This system consists of oxidation and reduction reactors where metal oxide particles circulate through these two reactors. The metal or partially oxidized metal oxide particles are oxidized with air in an air reactor, and the oxidized metal oxide particles are reduced by fuel in a fuel reactor. Separation of two reaction zones makes it possible to concentrate CO_2 from flue gas, and indirect combustion at lower temperatures does not produce thermal NO_x. At complete conversion of the fuel gas, the exit gas stream from the fuel reactor contains only CO_2 and H_2O; thereby, pure CO_2 can be obtained with H_2O condensation. The flue gas from the air reactor contains only N_2 and unreacted O_2. The extent of the reactions may vary depending on the metal oxides and the reaction conditions. The advantages of this system as compared to the normal combustion system are that CO_2 and H_2O are inherently separated from the rest of the flue gases, and no energy is expended for this separation.[2]

As shown in Figure 1, the CLC system is composed of two reactors, an air and a fuel reactor. The gaseous fuel is introduced into the fuel reactor where it reacts with an oxygen carrier particle as

$$(2n + m)\mathrm{Me}_x\mathrm{O}_y + \mathrm{C}_n\mathrm{H}_{2m} \rightarrow (2n + m)\mathrm{Me}_x\mathrm{O}_{y-1} + n\mathrm{CO}_2 + m\mathrm{H}_2\mathrm{O} \quad (1)$$

The reduced metal oxide is then circulated to the air reactor where it is oxidized according to

$$2\mathrm{Me}_x\mathrm{O}_{y-1} + \mathrm{O}_2 \rightarrow 2\mathrm{Me}_x\mathrm{O}_y \quad (2)$$

The total amount of heat evolved from reactions 1 and 2 would be the same as the normal combustion where O_2 is in direct contact with the fuel.

The CLC reactors (Figure 1) could be designed by two interconnecting fluidized beds that have an advantage over the other alternative designs since the process requires good contact between gas and solid phases and continuous smooth flow of solid materials between the two reactors.[3] A CFB combustor is considered as the CLC reactor since CFB has excellent gas−solid mixing characteristics. The reactivity of various oxygen carrier particles has been studied to find suitable metal oxides for higher conversion. However, the effective carrier particles are rather expensive chemical agents so that cheaper oxygen carrier materials are needed for large-scale power plants more than 10 MW. In the present study, the chosen metal oxides are NiO and Fe_2O_3, which are are supported on bentonite, TiO_2, or Al_2O_3. The reactivity of the selected metal oxides under the alternating conditions of reduction by CH_4 and oxidation by

* To whom correspondence should be addressed. Tel.: 82-42-869-3913. Fax: 82-42-869-3910. E-mail: kimsd@kaist.ac.kr.

10.1021/ie050919x CCC: $33.50
Published on Web 03/18/2006

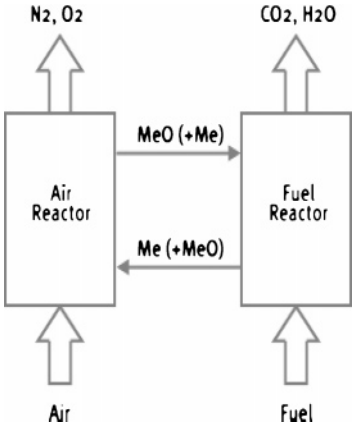

Figure 1. Schematic diagram of chemical-looping combustion.[1]

O_2 were determined in a thermobalance reactor. The CLC experiment was carried out in an annular shape circulating fluidized bed (CFB) reactor. It is composed of two bubbling fluidized bed zones in the core and annular sections and two risers where the oxygen carrier particles are circulated through each section. In the present study, the air reactor was also designed as a bubbling fluidized bed to provide enough reaction time since the oxidation reaction cannot be completed in the fast fluidized bed riser. This reactor system may provide enough residence or reaction time for each reaction, and the product gas can be separated from the each section. To optimize heat transfer from the oxidation (exothermic) to the reduction reactors (endothermic), an annular shape reactor was designed. Four different combinations of NiO and Fe_2O_3 supported on bentonite (NiO/Fe_2O_3 = 100:0, 75:25, 50:50, and 0:100) were prepared and tested. A mixture of NiO and Fe_2O_3 (75:25) on the bentonite support was examined to determine the optimum reaction temperature and fuel gas velocity.

Experimental Procedures

Reactivity of Oxygen Carrier Particles. NiO and Fe_2O_3 were used as the oxygen carriers, and bentonite, TiO_2, and Al_2O_3 were used as the supports. Those particles were prepared by the direct mixing of fine metal oxides whose size is less than 10 μm. The ratio of the carrier/support was 3:2, and distilled water was added into the well-mixed metal oxide particles to form a paste. The paste was dried at 383 K for 24 h and calcined at 1273 K for 6 h. Then, it was crushed and sieved for preparing a particle size range of 106−150 μm. The metal oxides with different supports (NiO/TiO_2, Fe_2O_3/TiO_2, NiO/Al_2O_3, and Fe_2O_3/Al_2O_3) and five different combinations of NiO and Fe_2O_3 supported on bentonite (NiO/Fe_2O_3 = 100:0, 75:25, 50:50, 25:75, and 0:100) were prepared.

Experiments were carried out in a thermobalance reactor (0.055 m i.d. × 1.0 m height). The experimental system consisted of two sections, reactor and weight detector, and the details of the thermobalance reactor can be found elsewhere.[4]

The reactor was heated to the desired temperature under N_2 flow initially, and then N_2 gas changed to the reaction gas, air, or CH_4. A metal oxide sample (3 g) was placed in a sampling basket suspended from an electronic balance and lowered down into the reaction zone using a motor-driven winch assembly with a reaction gas flow rate of 50 mm/s at 923−1223 K. The sample was exposed to a reducing gas (10% CH_4, 10% H_2O, 5% CO_2, and 75% N_2) to simulate the same atmosphere in the fuel reactor. The reduced sample was oxidized by 10% O_2. The reactant gas concentrations during the reducing (10% CH_4) and oxidizing periods (10% O_2) were chosen to simulate the average concentrations of the gases that may be exposed in a real CLC system.[5] After each reaction, the sample basket was elevated up to the hatch region and quenched.

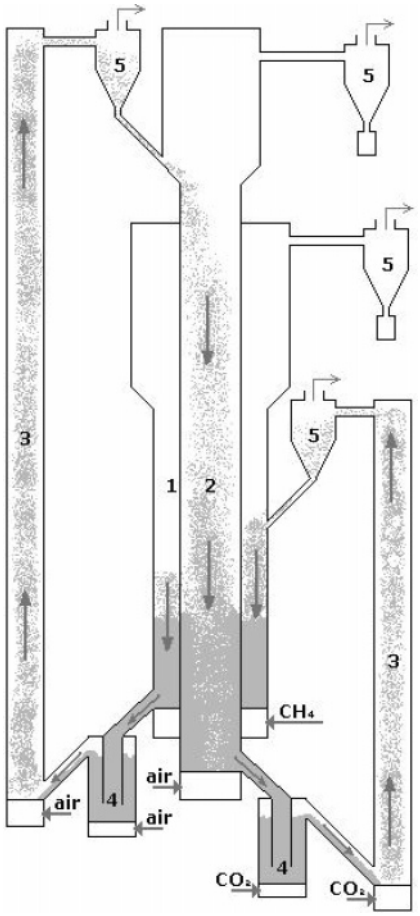

Figure 2. Schematic diagram of CFB reactor for CLC. (1) Reduction zone, annular column, 55 mm i.d., 0.9 m height; (2) oxidation zone, inner column, 23 mm i.d., 1.5 m height; (3) riser, 17 mm i.d., 2.1 m height for oxidizer, 1.15 m height for reducer; (4) loop-seal, 23 mm i.d., seal-pot type; and (5) cyclone.

Experimental Conditions in a Circulating Fluidized Bed (CFB) Reactor. A CFB combustor was considered the CLC reactor since CFB has excellent gas−solid mixing characteristics. The previous CFB systems for CLC are mostly composed of a high velocity riser and a low velocity bubbling fluidized bed.[1,6] The bed material circulating between the two fluidized beds is the O_2 carrier in the form of metal oxide particles. In the air reactor, or the riser, O_2 is transferred from the combustion air to the O_2 carrier. In the lower velocity fluidized bed, or the fuel reactor, O_2 is transferred from the carrier particles to the fuel. The gas velocity in the riser provides a driving force for circulating particles between the two fluidized beds. Thus, the particles carried away from the riser are recovered by a cyclone and led to the fuel reactor.

In the present study, however, the air reactor was also designed as a bubbling fluidized bed since the oxidation reaction was not sufficiently fast to complete the oxidation reaction in the fast fluidized bed riser.[5,7] To optimize heat transfer from the oxidation (exothermic reaction) reactor to the reduction (endothermic reaction) reactor, an annular shape reactor was designed as shown in Figure 2. To transport oxygen carrier particles between two sections, two risers were needed. One was for transporting the particles from the oxidation to the reduction zone and another riser provided the particle transport

from the reduction to the oxidation reactors. The design values and constants are adopted from the theoretical equations of Lyngfelt and coworkers[1] and Ryu and Jin.[6] The loop-seal is a kind of nonmechanical solid feeding control valve with a variation of aeration velocity, and the seal-pot type was adopted for the present reactor. Dimensions of the two loop-seals are the same based on the study of Basu and co-workers.[8]

The design criteria were based on a layout of an atmospheric boiler.[1,6] The design data and parameters were chosen according to the following considerations: (1) the fuel was CH_4 since natural gas is a suitable fuel for the CLC application. (2) The fuel gas flow in the reduction zone was kept at near minimum fluidized bed conditions for complete combustion of CH_4, and the gas flow into the oxidation zone was controlled for sufficient O_2 supply. (3) The temperature of the oxidation zone was a function of temperature in the reduction zone. (4) The oxygen carrier was NiO−Fe_2O_3/bentonite in the size range of 106−150 μm.

The oxygen carrier particles in the two bubbling beds were fed through each loop-seal and transported through each riser by aeration. The particles entering each riser were transported by high gas velocities to another reaction region. Thereby, the particles circulated between the oxidation and the reduction reactors, repeatedly.

The reactor was heated to a desired temperature and then reactant gases, air and CH_4, were introduced into each reactor. In the loop-seals, CO_2 and air were used to aerate particles for smooth solid circulation, the same gases at a velocity around 1.5 m/s were supplied into the risers for solid transportation, and the solid circulation rate was around 13 kg/m^2 s. The metal oxides were loaded in both the reaction zones, 0.6 kg in the reduction reactor and 0.2 kg in the oxidation reactor. The bed weights and solid circulation rate were estimated by residence time for the complete reaction. The present chemical-looping combustion with four different combinations of NiO and Fe_2O_3 supported on bentonite was carried out at 923−1223 K. The fuel gas, CH_4, was introduced into the reduction reactor in a range of 25−100 mm/s (i.e., 1−4 u_{mf}). The sampled flue gas was analyzed by gas chromatography (HP GC 5890 series II) with a thermal conductivity detector and columns of Molecular Sieve 5A and Porapak Q. To calculate the amount of product gas and its composition from the reduction reactor, argon gas as a tracer was injected into the reactor.

Results and Discussion

Properties of Oxygen Carrier Particles. The chemical structures of the samples were characterized by using X-ray powder diffraction (Bruker D8Discover GADDS CS, Cu Kα radiation). The O_2 carriers of dual metal oxides (NiO−Fe_2O_3/bentonite) were composed of a Ni−Fe alloy oxide, $NiFe_2O_4$. The particles supported on TiO_2 were composed of $NiTiO_3$ or Fe_2TiO_5 as found in a previous study.[9] Since bentonite is a complex material with SiO_2, Al_2O_3, and lots of other metal oxides, X-ray diffraction patterns of the particles on bentonite cannot be seen as a significant crystalline phase of the support, and only NiO or Fe_2O_3 can be found; the crystalline phases of the particles are illustrated in Table 1.

Actual loading of NiO and Fe_2O_3 was based on the inductively coupled plasma-mass spectroscopy (ICP-MS) data and the uniformity of NiO distribution that was determined by Ni mapping through energy-dispersive X-ray spectrometry (EDS, EDAX Int. Corp.; 20 keV). Because the raw materials are not pure ones used for industrial application, actual loadings were below 60 wt %. However, Fe_2O_3 loading on bentonite was above the expected values that may be caused by inherent Fe_2O_3 in the bentonite. It was found that NiO was distributed uniformly throughout bentonite from the Ni mapping image of NiO/bentonite, and it may be expected that the other metal oxides would be the same. Also, the Ni mapping image of the NiO/bentonite particle can be seen in Figure 3.

Table 1. Main Crystalline Phase of Fresh Oxygen Carrier Particles

specimen	main crystalline phase
NiO/TiO_2	NiO, $NiTiO_3$
Fe_2O_3/TiO_2	Fe_2O_3, Fe_2TiO_5
NiO/Al_2O_3	NiO, Al_2O_3
Fe_2O_3/Al_2O_3	Fe_2O_3, Al_2O_3
NiO/bentonite (NiO/Fe_2O_3 = 100:0)	NiO
NiO−Fe_2O_3/bentonite (NiO/Fe_2O_3 = 75:25)	$NiFe_2O_4$, NiO, Fe_2O_3
NiO−Fe_2O_3/bentonite (NiO/Fe_2O_3 = 50:50)	$NiFe_2O_4$, NiO, Fe_2O_3
NiO−Fe_2O_3/bentonite (NiO/Fe_2O_3 = 25:75)	$NiFe_2O_4$, NiO, Fe_2O_3
Fe_2O_3/bentonite (NiO:Fe_2O_3 = 0:100)	Fe_2O_3

Reaction Kinetics of Oxygen Carrier Particles. The reduction and oxidation of different oxygen carrier particles on different supports at 1123 K are shown in Figure 4 where the fractional oxidation is defined as

$$X = \frac{m - m_{red}}{m_{ox} - m_{red}} \tag{3}$$

where m, m_{red}, and m_{ox} are, respectively, weight of the sample, weight of the sample after being fully reduced, and weight of the sample after being fully oxidized. The values of m_{red} are determined to be metallic Ni and Fe since they can be reduced with the strong reducing conditions.

As can be seen, the reactivity of NiO is faster than Fe_2O_3 regardless of the supports. The reduction conversion of Fe_2O_3 is not high enough just over 0.7. The particles supported on bentonite or Al_2O_3 exhibit higher reactivity than those on TiO_2. The conversion of the particles on Al_2O_3 is 2 times faster than that on bentonite to reach a 100% conversion of oxidation. The particles on the TiO_2 support exhibit lower conversion. The particles on bentonite do not produce a high reaction rate**,** but they continue with the fractional oxidation down to 0.1 after 10 min as was found previously.[10] Since oxidation conversion of the selected metal oxides on the bentonite support reaches 100%, these metal oxides on that support can be utilized for the CLC system with a two-stage bubbling fluidized bed reactor. However, NiO/Al_2O_3 cannot be utilized for CLC in a CFB reactor due to their low crushing strength as found in the present and previous studies.[7,11] On the basis of the reactivity test, NiO and Fe_2O_3 supported on bentonite were selected for the kinetic study. Five different kinds of NiO−Fe_2O_3/bentonite particles were prepared with different loading ratios. The reactivity increases with increasing reaction temperature and the amount of NiO.

The reaction rate (dX/dt) is defined as

$$\frac{dX}{dt} = -\frac{1}{m}\frac{dm}{dt} \tag{4}$$

For modeling the present gas−solid reaction kinetics, three different gas−solid reaction models, namely, the shrinking core, uniform reaction, and modified volumetric models,[12,13] have been adopted.

The reaction kinetics for the shrinking core model is represented by

$$\frac{dX}{dt} = k_r(1 - X)^{2/3} \tag{5}$$

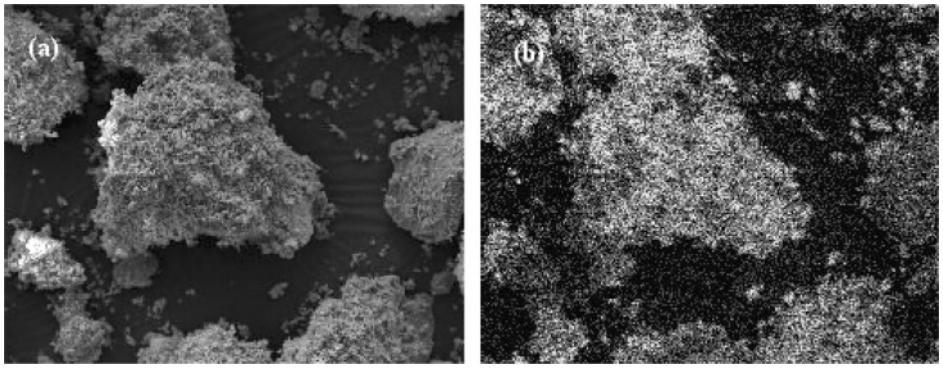

Figure 3. EDS image of NiO/bentonite particle. (a) Original SEM image and (b) Ni mapping image.

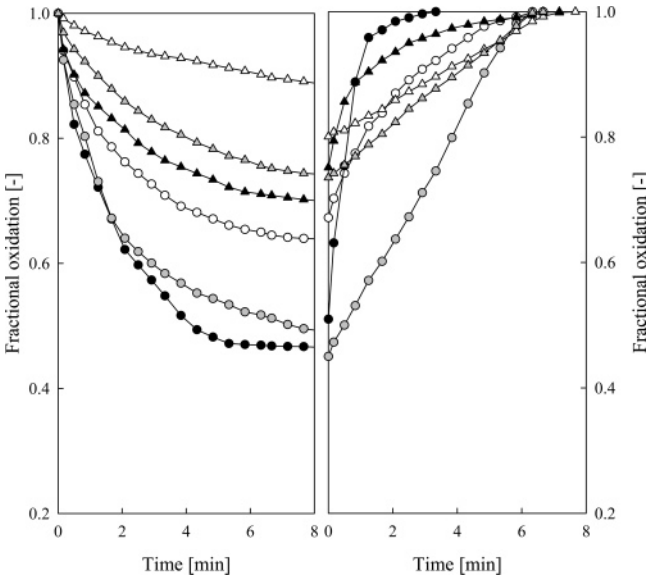

Figure 4. Fractional reduction and oxidation with time. (a) Reduction; (b) oxidation; ○ NiO/TiO_2; ● NiO/Al_2O_3; gray circle NiO/bentonite; △ Fe_2O_3/TiO_2; ▲ Fe_2O_3/Al_2O_3; and gray triangle Fe_2O_3/bentonite.

From eq 5, the reaction constant can be derived as

$$k_r = \frac{3}{t}\{1 - (1 - X)^{1/3}\} \tag{6}$$

Reaction kinetics for the uniform reaction model and its reaction constant are as follows

$$\frac{dX}{dt} = k_v(1 - X) \tag{7}$$

$$k_v = -\frac{1}{t}\ln(1 - X) \tag{8}$$

For the modified volumetric model, the experimental data ($X - t$) can be expressed as the following equation, and the values of the constants a and b are determined by the least-squares method.

$$X = 1 - \exp(-at^b) \tag{9}$$

The reaction rate for the modified volumetric model is derived as

$$\frac{dX}{dt} = a^{1/b}b[-\ln(1 - x)]^{(b-1)/b}(1 - X) \tag{10}$$

The reaction constant (k_m) can be determined when the conversion is 0.5, and the reaction kinetics is expressed as follows:

$$k_m \approx k_x|_{X=0.5} = a^{1/b}b(\ln 2)^{(b-1)/b} \tag{11}$$

$$\frac{dX}{dt} = k_m(1 - X) \tag{12}$$

For the reduction and oxidation reaction kinetics of five different combinations of $NiO-Fe_2O_3$/bentonite particles, three gas−solid reaction models were applied. Among the three models, it has been found that the modified volumetric model is the best representation of the reduction of $NiO-Fe_2O_3$/bentonite particles. The agreement between the experimental data and the modified volumetric model is shown in Figure 5 for the reduction of the $NiO-Fe_2O_3$/bentonite (NiO/Fe_2O_3 = 50:50) particle.

The activation energies and preexponential factors of each particle system were determined from the Arrhenius plot (Figure 6), and the obtained activation energies and preexponential factors of each particle system are shown in Figure 7. The obtained values are correlated as a function of the Fe_2O_3 ratio ($R_{Fe_2O_3}$) in $NiO-Fe_2O_3$ as shown in eqs 13−15. $R_{Fe_2O_3}$ is a percent value of the Fe_2O_3 ratio when the sum of NiO and Fe_2O_3 is 100%. The activation energies and preexponential factors of five kinds of $NiO-Fe_2O_3$/bentonite particles are correlated with $R_{Fe_2O_3}$ with correlation coefficients of 0.995 and 0.984, respectively, as

$$\frac{dX}{dt} = a_{red}\exp\left(\frac{-E_{a,red}}{RT}\right)(1 - X) \tag{13}$$

$$a_{red} = 2.05 \times 10^{-1} + 3.93 \times 10^{-3} R_{Fe_2O_3} + 1.96 \times 10^{-5} R_{Fe_2O_3}{}^2 \text{ (for } R_{Fe_2O_3} > 25) \tag{14}$$

$$E_{a,red} = 5.71 \times 10 - 5.62 \times 10^{-1} R_{Fe_2O_3} + 2.79 \times 10^{-3} R_{Fe_2O_3}{}^2 \tag{15}$$

It has been found that the oxidation reactivity of $NiO-Fe_2O_3$/bentonite can be represented by both the shrinking core and the uniform reaction models. From the agreement between experimental data and both models, the shrinking core model is little better representation of the data than the uniform reaction model for the oxidation of $NiO-Fe_2O_3$/bentonite particles.

The agreements between the experimental data and those from the model equations are shown in Figure 8 for the oxidation of $NiO-Fe_2O_3$/bentonite (NiO/Fe_2O_3 = 50:50) particles. Again, the activation energies and preexponential factors for each particle for oxidation were determined from the Arrhenius plot (Figure 9). As can be seen, the reaction kinetics exhibit different patterns below and above 1073 K.

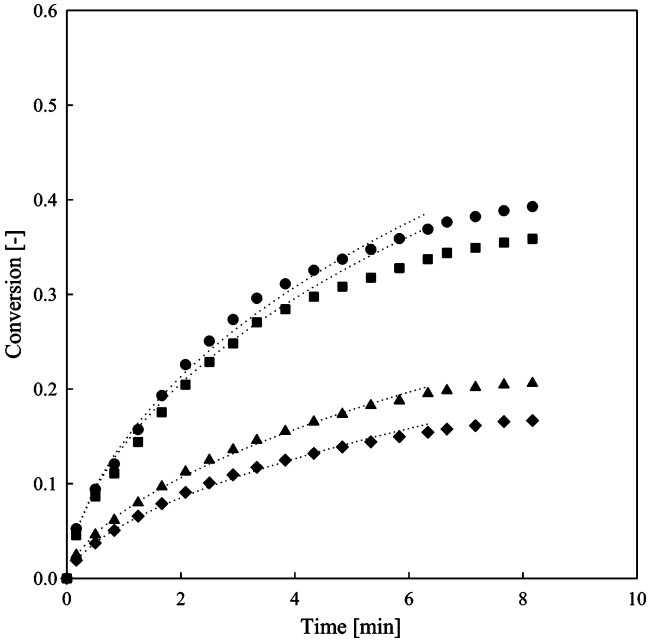

Figure 5. Comparison between the experimental data and the modified volumetric model for reduction of NiO−Fe_2O_3/bentonite (NiO/Fe_2O_3 = 50:50) particle. (● 1223 K; ■ 1123 K; ▲ 1023 K; and ◆ 923 K.)

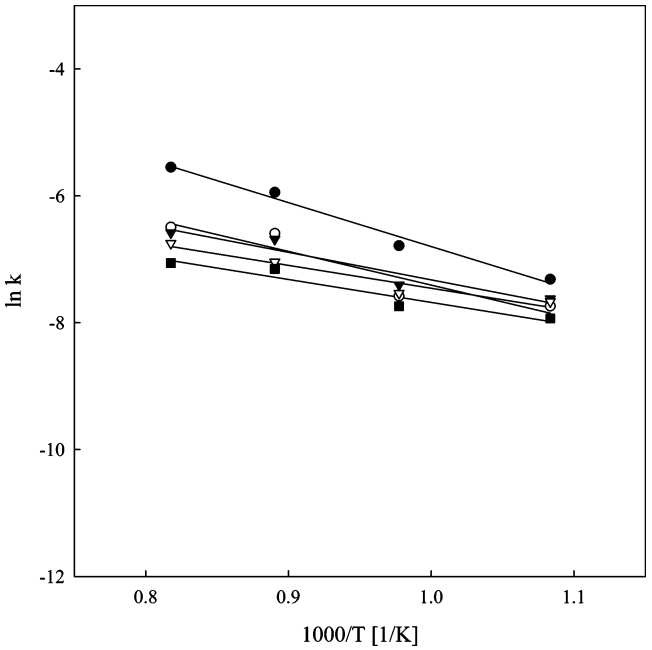

Figure 6. Arrhenius plot of reduction of each NiO−Fe_2O_3/bentonite particle from the modified volumetric model. (NiO/Fe_2O_3 = ● 100:0; ○ 75:25; ▼ 50:50; □ 25:75; and ■ 0:100.)

The obtained activation energies and preexponential factors for each particle for oxidation are correlated as a function of $R_{Fe_2O_3}$ as shown in eqs 16−18, and those data are shown in Figure 10. Since the temperature in the real CLC operation is higher than 1073 K, those data in the temperature range above 1073 K in the Arrhenius plot are chosen for the correlation, and the correlation coefficients are 0.996 and 0.908, respectively.

$$\frac{dX}{dt} = a_{ox} \exp\left(\frac{-E_{a,ox}}{RT}\right)(1 - X)^{2/3} \quad (16)$$

$$a_{ox} = 3.73 \times 10^{-3} - 7.79 \times 10^{-6} R_{Fe_2O_3} \quad (17)$$

$$E_{a,ox} = 2.40 + 3.60 \times 10^{-2} R_{Fe_2O_3} \quad (18)$$

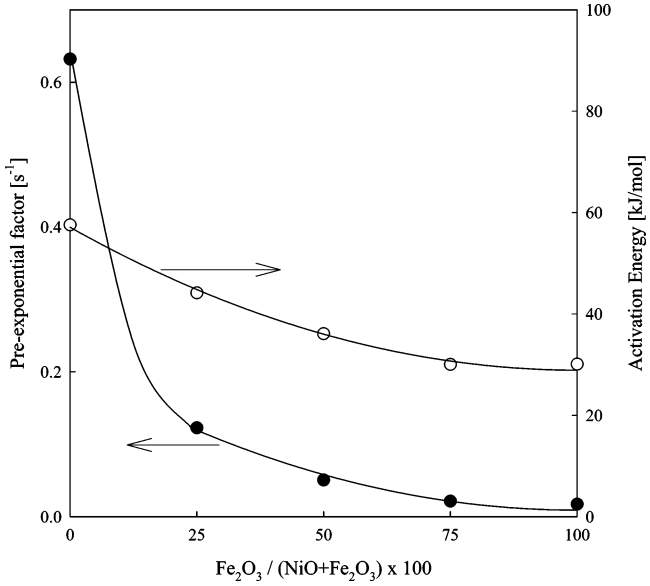

Figure 7. Preexponential factors and activation energies for reduction of each NiO−Fe_2O_3/bentonite particle. (● preexponential factor and ○ activation energy.)

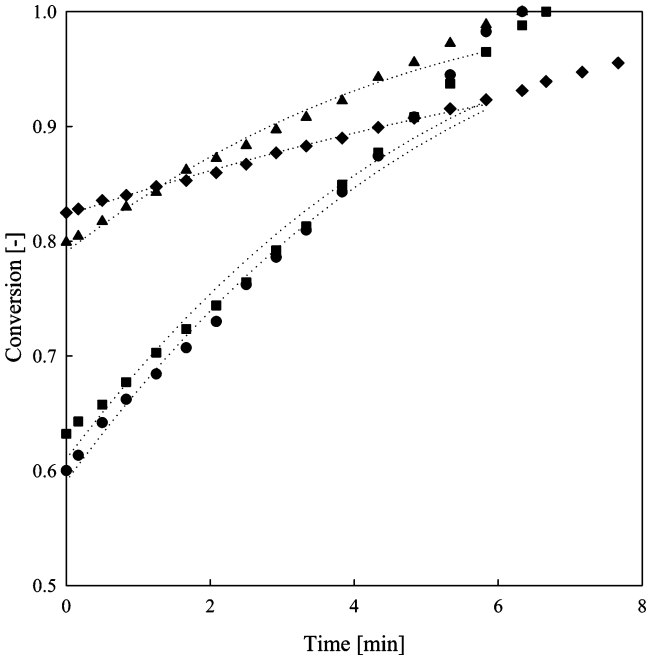

Figure 8. Comparison between the experimental data and the shrinking core model for oxidation of NiO−Fe_2O_3/bentonite (NiO/Fe_2O_3= 50:50) particle. (● 1223 K; ■ 1123 K; ▲ 1023 K; and ◆ 923 K.)

The difference between the reduction and the oxidation reactions may be attributed to the following reasons. For the reduction and oxidation reactions, the chemical composition of the oxygen carrier particles and support materials may control the reaction velocity. Therefore, the uniform reaction model is also well-fitted to the data of oxidation. However, reactive sites on which the reaction is active may control the oxidation kinetics. On the basis of the obtained data, the reduction and oxidation of NiO−Fe_2O_3/bentonite particles may be controlled by the chemical composition strongly, but after the reaction starts, the reactive site would be also an important factor for the reaction velocity.

Reactivity in the Circulating Fluidized Bed Reactor with Double Loops. The CLC in the CFB reactor was characterized by analyzing the flue gas. If the desired reaction occurs, only

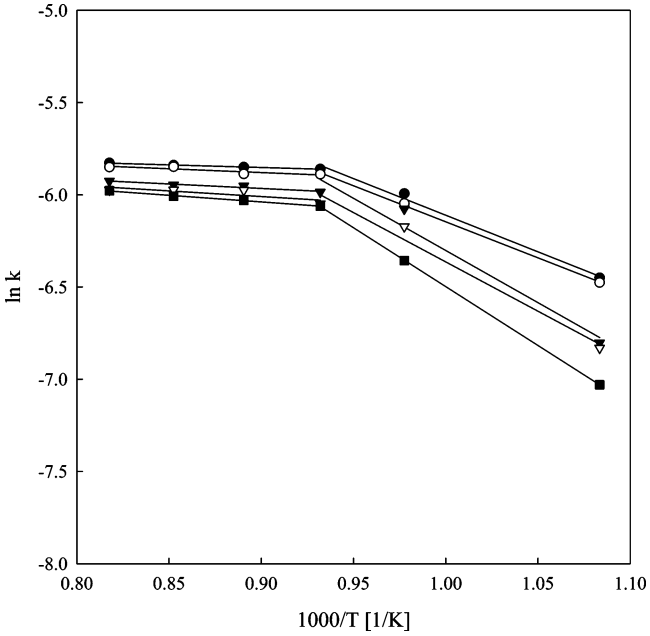

Figure 9. Arrhenius plot of oxidation of each NiO−Fe_2O_3/bentonite particle from the shrinking core model. (NiO/Fe_2O_3 = ● 100:0; ○ 75:25; ▼ 50:50; □ 25:75; and ■ 0:100.)

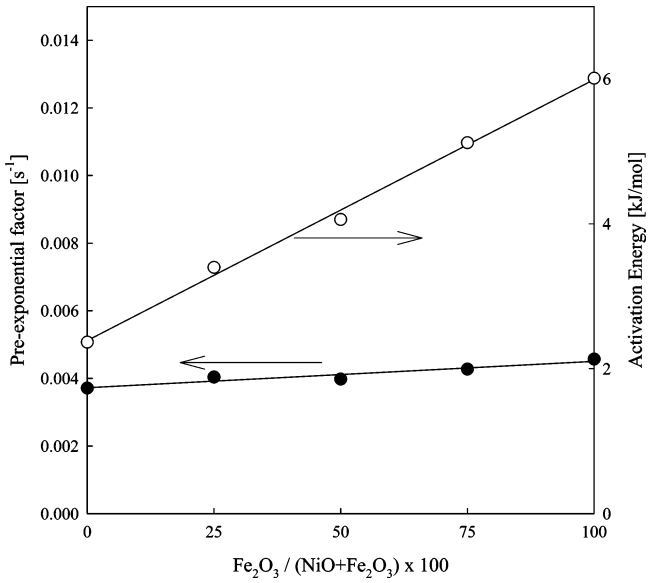

Figure 10. Preexponential factors and activation energies of oxidation for each NiO−Fe_2O_3/bentonite particle. (● preexponential factor and ○ activation energy.)

CO_2 and H_2O would be detected in the flue gas from the reduction reactor. However, CO and H_2 may be formed by the side reactions in the reduction reactor and NO_x from the oxidation reactor. The injected fuel, CH_4, could be emitted due to the incomplete reduction reaction. Using a ND-IR type NO analyzer, NO_x from the oxidation reactor was detected only several ppm within the error boundary. It may imply that the thermal NO_x emission is negligibly small. The reaction efficiency can be determined by the analysis of flue gas from the reduction reactor. The possible composition of the flue gas is mixtures of CO_2, CO, H_2, and CH_4. On the basis of the analyzing data, most of CH_4 was converted to CO_2, and several percentages of CO were detected by the side reaction. In some cases, CH_4 was emitted without conversion. H_2 was not analyzed. In a batch reactor mode, CO and H_2 were detected strongly; however, CO and H_2 were detected less in a continuous CFB reactor since the excess oxidized metal oxide particles may react completely with the supplied CH_4 gas.

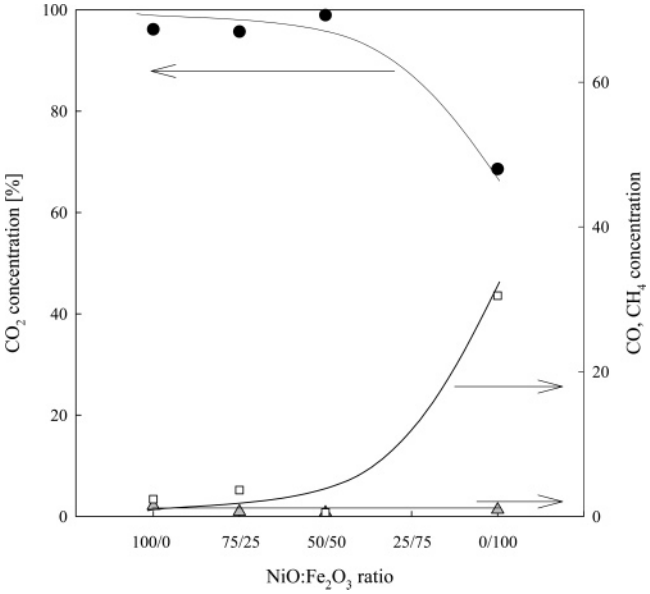

Figure 11. Effect of NiO/Fe_2O_3 on the product gas composition at 1123 K and CH_4 velocity = 50 mm/s (● CO_2; ▲ CO; and □ CH_4.)

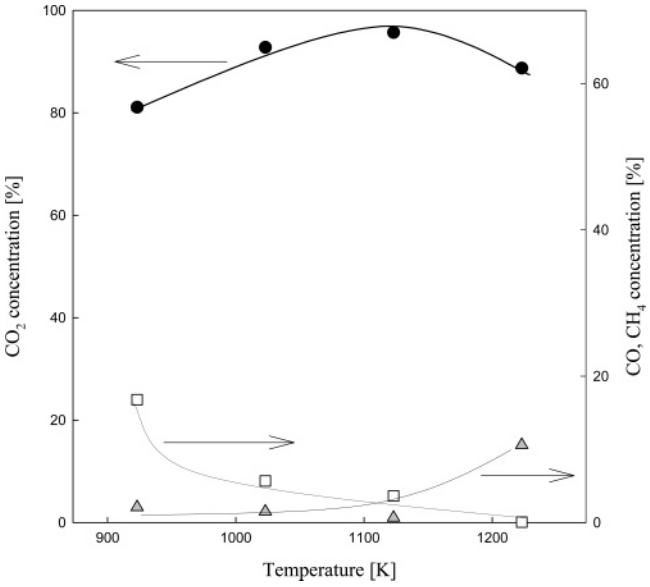

Figure 12. Effect of temperature on the product gas composition with NiO−Fe_2O_3/bentonite (NiO/Fe_2O_3 = 75:25) and CH_4 velocity = 50 mm/s. (● CO_2; ▲ CO; and □ CH_4.)

The effect of the NiO/Fe_2O_3 ratio on the product gas in the reduction reactor is shown in Figure 11. As can be seen, methane is combusted almost completely, over 95% with the content of NiO above 50%. The reactivity of the oxygen carrier particles increases with increasing NiO content. With the Fe_2O_3/bentonite, 30% of CO was emitted, which indicates that Fe_2O_3 cannot transfer O_2 sufficiently as found in our previous reactivity study.[7] Unreacted methane was not detected in all cases studied. With these results, it is found that complete CH_4 conversion is obtained with the employed oxygen carrier particles and that the O_2 carrying capacity decreases with increasing Fe_2O_3 content. From the reactivity experiment, NiO/bentonite is the best choice for CLC application, but based on cost and the attrition tests,[7] the optimum ratio of NiO/Fe_2O_3 is found to be 3 (NiO/Fe_2O_3 = 75:25).

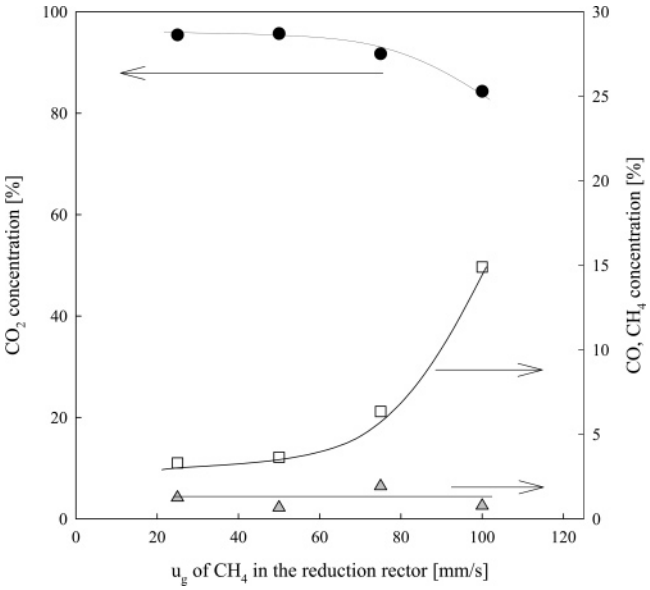

Figure 13. Effect of methane velocity on the product gas composition at 1123 K and with NiO−Fe_2O_3/bentonite (NiO/Fe_2O_3 = 75:25). (● CO_2; ▲ CO; and □ CH_4.)

The effect of reaction temperature on the product gas composition is shown in Figure 12. As can be seen, concentration of CO_2 increases with increasing reaction temperature. Unreacted methane increases with decreasing reaction temperature, while CO emission increases with increasing temperature. At higher temperatures, the side reactions may accelerate in both reaction regions to have enough energy for the reaction activation. With these data, it can be found that the optimum reaction temperature is around 1123 K.

The effect of methane velocity on the product gas in the reduction reactor is shown in Figure 13. As can be seen, unreacted CH_4 increases with increasing methane velocity. It was observed that CH_4 emission increases significant at gas velocity above 75 mm/s by the excess injection of CH_4. Therefore, the optimum CH_4 velocity would be around 50−70 mm/s (2−3 u_{mf}) in the present reactor system.

Conclusion

The reactivity of the oxygen carrier particles (NiO and Fe_2O_3) with different supports (TiO_2, Al_2O_3, and bentonite) were determined in a thermobalance reactor at alternating reduction and oxidation conditions at 1123 K. The reactivity of NiO is higher than that of Fe_2O_3, and the particles supported on bentonite or Al_2O_3 produce higher reactivity than those on TiO_2. The reactivity of the oxygen carrier particles increases with increasing reaction temperature and the amount of NiO. The obtained conversion data in the reduction condition can be represented by the modified volumetric model, whereas the conversion data in the oxidation condition is well-represented by the shrinking core model.

The CLC experiment was carried out in an annular shape CFB reactor with four different combinations of NiO and Fe_2O_3 supported on bentonite. It is found that CO emission from the fuel reactor is very small and that no H_2 emission was detected. From the oxidation reactor, the NO_x emission is also negligibly small, and the CO_2 emission cannot be detected in the present reactor system. The reactivity of the carrier particles increases with increasing NiO content, but the optimum ratio of NiO/Fe_2O_3 was found to be 3 (NiO/Fe_2O_3 = 75:25) based on their price and the attrition test. The combustion efficiency increases with an increasing reaction temperature, and its optimum temperature is found to be 1123 K. The conversion of CH_4 is higher at lower CH_4 velocities, and the optimum CH_4 velocity for complete combustion is around 2−3 u_{mf}.

Acknowledgment

We acknowledge a grant-in-aid for research to S.D.K. from the Research and Development Program for Electric Power Industry (R-2002-0-263-0-00), which is funded by the Ministry of Commerce, Industry and Energy, Korea.

Nomenclature

a = constant determined by curve fitting using the least-square method with conversion (X) and time (t)
a_{ox} = pre-exponential factor for oxidation (s^{-1})
a_{red} = pre-exponential factor for reduction (s^{-1})
b = constant determined by curve fitting using the least-square method with conversion (X) and time (t)
$E_{a,ox}$ = activation energy for oxidation (kJ/mol)
$E_{a,red}$ = activation energy for reduction (kJ/mol)
k_m = rate constant in modified volumetric model (s^{-1})
k_r = rate constant in shrinking core model (s^{-1})
k_s = specific rate constant in a fixed-bed reactor (s^{-1})
k_v = rate constant in uniform reaction model (s^{-1})
m = actual mass of O_2 carrier sample (g)
m_{ox} = mass of O_2 carrier sample when fully oxidized (g)
m_{red} = mass of O_2 carrier sample when fully reduced (g)
R = gas constant (J/kg mol K)
$R_{Fe_2O_3}$ = Fe_2O_3 ratio in NiO−Fe_2O_3
T = reaction temperature (K)
t = time (s)
u_g = gas velocity in a fluidized bed (mm/s)
u_{mf} = minimum fluidizing velocity (mm/s)
X = fractional oxidation of oxygen carrier or conversion (eq 3)

Literature Cited

(1) Lyngfelt, A.; Leckner, B.; Mattison, T. A Fluidized-bed Combustion Process with Inherent CO_2 Separation; Application of Chemical-Looping Combustion. *Chem. Eng. Sci.* **2001**, *56*, 3101−3113.

(2) Richter H. J.; Knoche, K. F. *Reversibility of Combustion Process*; ACS Symposium Series, American Chemical Society: Washington, DC, 1983; pp 71−85.

(3) Ishida, M.; Zheng, D.; Akehata, T. Evaluation of a Chemical-Looping Combustion Power-Generation System by Graphic Exergy Analysis. *Energy* **1987**, *12* (2), 147−154.

(4) Song, B. H.; Kim, S. D. Catalytic Activity of Alkali and Iron Salt Mixtures for Steam-Char Gasification. *Fuel* **1993**, *72*, 797−803.

(5) Mattison, T.; Järdnäs, A.; Lyngfelt, A. Reactivity of Some Metal Oxides Supported on Alumina with Alternating Methane and Oxygen-Application for Chemical-Looping Combustion. *Energy Fuels* **2003**, *17*, 643−651.

(6) Ryu, H. J.; Jin, G. T. Conceptual Design of 50 kW Thermal Chemical-Looping Combustor and Analysis of Variables. *Energy Eng. J.* **2003**, *12* (4), 289−301.

(7) Son, S. R.; Kim, S. D. *Reactivity and Attrition Characteristics of Oxygen Carrier Particles for Chemical-Looping Combustion*, ISTP 2004; 3rd International Symposium on Two-Phase Flow Modeling and Experimentation: Pisa, Italy, September 22−24, 2004.

(8) Basu, P.; Fraser, S. A. *Circulating Fluidized Bed Boilers: Design and Operations*; Butterworth-Heinemann: Boston, 1991.

(9) Jin, H.; Okamoto, T.; Ishida, M. Development of a Novel Chemical-Looping Combustion: Synthesis of a Solid Looping Material of NiO/$NiAl_2O_4$. *Ind. Eng. Chem. Res.* **1999**, *38*, 126−132.

(10) Son, S. R.; Kim, S. D. *Carbon Deposition and Carbide Formation by Reduction of Metal Oxides Using Methane*; Presented at the 16th Symposium on Chemical Engineering Daejeon/Chungnam (Korea) and Kyushu (Japan): Daejeon, Korea, December 5−6, 2003.

(11) Adánez, J.; de Diego, L. F.; García-Labiano, F.; Gayán, P.; Abad, A. Selection of Oxygen Carriers for Chemical-Looping Combustion. *Energy Fuels* **2004**, *18*, 371−377.

(12) Levenspiel, O. *Chemical Reaction Engineering*, 3rd ed.; Wiley: New York, 1999.

(13) Kasaoka, S.; Skata, Y.; Tong, C. Kinetic Evaluation of the Reactivity of Various Coal Chars for Gasification with Carbon Dioxide in Comparison with Steam. *Ind. Chem. Eng.* **1985**, *25* (1), 160−175.

Received for review August 9, 2005
Revised manuscript received December 20, 2005
Accepted December 22, 2005

IE050919X